JOURNAL OF MATERIALS SCIENCE 19 (1984) 3976–3986

On the work hardening behaviour of metallic materials with spherical second-phase particles at high temperatures

MANABU TANAKA, HIROSHI IIZUKA
Department of Mechanical Engineering for Production, Mining College of Aikita University, Akita 010, Japan

The work hardening behaviour of metallic materials with spherical second-phase particles at elevated temperatures has been discussed theoretically, based on the continuum mechanics model which incorporated the effect of the dynamic recovery by diffusion of atoms. It was found that the theoretical model developed in this study could satisfactorily explain the experimental results of tensile tests in an austenitic heat-resisting steel with $M_{23}C_6$ carbides. The model was also applied to the understanding of the internal stress during high-temperature creep in this steel.

1. Introduction

Theoretical discussions based on continuum mechanics have recently been made on the temperature dependence of work hardening due to second-phase particles in metallic materials. Mori and co-workers [1, 2] and Matsuura [3, 4] have discussed the mechanisms of static and dynamic recovery in the dispersion strengthened metals below about $0.4T_m$ (T_m is the melting point of base metal), where the pipe diffusion is considered to control the climb and annihilation of Orowan loops formed around particles during deformation.

At high temperatures above about $0.5T_m$, recovery and creep are controlled by volume diffusion or grain boundary diffusion of atoms. Ashby [5] theoretically discussed the particle size dependence of grain boundary sliding of dispersion-strengthened metals during creep in this temperature range. However, the dislocation structure around second-phase particles is generally so complex that a quantitative interpretation has not fully been made on the work hardening behaviour of the material at elevated temperatures.

In this study, temperature and particle size dependence of the work hardening at high temperatures (where volume diffusion of atoms controls the dynamic recovery, have been calculated using a continuum mechanics model. The result of the calculation based on this model was then compared with that of experiment for an austenitic heat-resisting steel with $M_{23}C_6$ carbides.

2. Calculation

The deformation of metallic materials with non-deforming spherical precipitates is considered. It is assumed that plastic deformation occurs only in the matrix under an external stress in the x_3-direction, σ_{33}^A ($\epsilon_{33}^* = \epsilon^*$, $\epsilon_{11}^* = \epsilon_{22}^* = -\epsilon^*/2$). The Gibbs free energy of the material owing to plastic deformation is given by [6]

$$G = \tfrac{3}{4}A\mu\epsilon^{*2}fV_0 + B\sigma_{33}^A\epsilon^* fV_0 + \sigma_0\epsilon^* V_0 - \sigma_{33}^A\epsilon^* V_0 + E_0(\sigma_{33}^A) \quad (1)$$

where μ is the rigidity of matrix, V_0 the total volume of the material, N the number of precipitate particles, V the volume of a particle, and $f = NV/V_0$. A and B are the shape factors which are functions of the rigidity and Poisson's ratio of the matrix and the precipitates. The first term in Equation 1 is the elastic strain energy, the second is the interaction energy between external stress and internal stress field, and the third is the energy dissipation due to plastic deformation in matrix, where σ_0 is the yield stress. The fourth term in Equation 1 is the decrease in external potential

0022–2461/84 $03.00 + .12

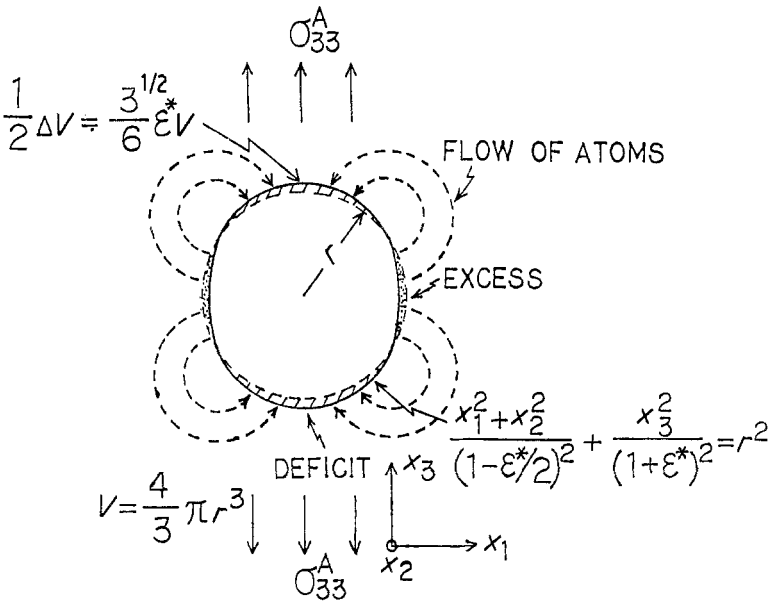

Figure 1 Schematic illustration of the accommodation of the misfit strain by diffusion of atoms in matrix.

owing to plastic deformation, and $E_0(\sigma_{33}^{A})$ is the energy term independent of ϵ^*. The interaction between precipitate particles is neglected, provided that $f \ll 1$.

From the stability of the system, $\partial G/\partial \epsilon^* = 0$ and $\partial^2 G/\partial \epsilon^{*2} > 0$ [6]. Therefore,

$$\sigma_{33}^{A} = \frac{3}{2} A\mu\epsilon^* \frac{f}{1-Bf} + \frac{f}{1-Bf}. \quad (2)$$

The amount of work hardening, $\Delta\sigma$, is given by

$$\Delta\sigma = \frac{3}{2} A\mu\epsilon^* \frac{f}{1-Bf}. \quad (3)$$

Substituting Equation 2 into Equation 1,

$$G = -\tfrac{3}{4} A\mu\epsilon^{*} f V_0 + E_0(\sigma_{33}^{A}) \quad (4)$$

$$A = \frac{2\mu'(7-5\nu)}{2\mu'(4-5\nu)+\mu(7-5\nu)}$$

and

$$B = \frac{15\mu'(1-\nu)}{2\mu'(4-5\nu)+\mu(7-5\nu)}$$

for spherical particles with the rigidity μ' and Poisson's ratio ν' which are different from the values of the matrix, μ and ν [7]. Work hardening of the material arises from back stress in the matrix induced by Orowan loops [3]. ϵ^* is identical with the measured plastic strain, ϵ, when neither annihilation of Orowan loops by climb nor plastic accommodation occurs.

No volume change occurs in plastic deformation; however, change in shape of the matrix around a precipitate particle (radius r) results in an excess of matrix volume, shown as the shaded part (or a deficit of volume as the hatched part) in Fig. 1. From the geometrical consideration, the total excess (or deficit) of volume, ΔV, is given by Equation 5, neglecting the terms of higher order in ϵ^*:

$$\Delta V \fallingdotseq \frac{3^{1/2}}{3} \epsilon^* V \quad (V = \tfrac{4}{3}\pi r^3) \quad (5)$$

Ashby [5] obtained $\gamma_p V/8$ as the value of $\Delta V/2$ for shear deformation (γ_p is plastic shear strain). A uniform distribution of dislocation loops around a particle is assumed in the present calculation, whereas the annihilation process of dislocation loops in each slip system is still unknown. It is considered that the change in Gibbs free energy of the material is caused by diffusion of atoms in the matrix, which accommodates the misfit strain between a particle and the matrix, and consequently leads to annihilation of dislocation loops. Further, the effects of the other accommodation processes such as cross-slip or formation of prismatic loops is neglected here. The number of atoms contained in V for ϵ^* and that for ϵ are, respectively, given by

$$n = \frac{\Delta V}{\Omega} \fallingdotseq \frac{3^{1/2}\epsilon^* V}{3\Omega} \quad (6)$$

$$n_0 \fallingdotseq \frac{3^{1/2}\epsilon V}{3\Omega} \quad (7)$$

where Ω is the atomic volume.

The Gibbs free energy of the system is also

expressed by Equation 8, substituting Equation 6 into Equation 4:

$$G = -\frac{9A\mu n^2\Omega^2}{4V} + E_0(\sigma_{33}^{A}) \quad (8)$$

If the free energy is changed by dG due to migration of atoms, dn, from the region of volume excess to that of volume deficit, the difference in chemical potential between the emission and absorption sides of atoms, μ^* (or in other words, the "force" acting on a migrating atom [8]), is given by

$$\mu^* = -\frac{dG}{dn} = \frac{9A\mu n\Omega^2}{2V} \quad (9)$$

The migration rate of atoms, (dn/dt), is then considered. Since the diffusion distance is approximately equal to the radius, r, of a spherical precipitate in this case, the flux of atoms is given by

$$J = \frac{D}{\Omega kT}\,\mathrm{grad}\,\mu^* = \frac{9A\mu n\Omega D}{2kTrV} \quad (10)$$

where k is Boltzmann's constant, T absolute temperature and D the diffusion constant. D in Equation 10 is given as D_v when the migration of atoms is controlled by volume diffusion. The total cross-section of diffusion is considered to be approximately πr^2, since stresses outside a particle fall off as $(r/R)^3$, where R is the distance from the particle centre. Further, the recovery process is considered to be controlled by grain boundary diffusion when the interface between a precipitate particle and matrix is a grain boundary or a non-coherent interface. The total cross-section of diffusion is approximately $2\pi r\delta$ (δ is the thickness of the grain boundary) and D should be replaced by D_{GB} for grain boundary diffusion. The migration rate of atoms for volume diffusion and that for grain boundary diffusion are, respectively, given by

$$\left(\frac{dn}{dt}\right)_v \fallingdotseq \pi r^2 J = \frac{9\pi r^2 A\mu n\Omega D_v}{2kTrV} = \frac{27A\mu n\Omega D_v}{8r^2kT} \quad (11)$$

$$\left(\frac{dn}{dt}\right)_{GB} \fallingdotseq 2\pi r\delta J = \frac{27A\mu n\Omega D_{GB}\delta}{4r^3kT} \quad (12)$$

The migration rate of atoms is proportional to r^{-2} for volume diffusion and to r^{-3} for grain boundary diffusion. This is consistent with the calculated result of Ashby [5].

In tensile tests of the material at elevated temperatures, an increment in excess (or deficit) of atoms with time, dn_0/dt, produced under a strain rate $\dot{\epsilon}(=d\epsilon/dt)$ is decreased by the diffusion-controlled recovery by $(dn/dt)_v$ or $(dn/dt)_{GB}$. The total migration rate for volume diffusion is given by

$$\frac{dn}{dt} = \frac{dn_0}{dt} - \left(\frac{dn}{dt}\right)_v \quad (13)$$

Differentiating Equation 7 with respect to t, and substituting the result together with Equation 11 into Equation 13, the total migration rate is also given by

$$\frac{dn}{dt} = \frac{3^{1/2}V\dot{\epsilon}}{3\Omega} - \frac{27A\mu\Omega D_v}{8r^2kT}n = \bar{B} - Cn \quad (14)$$

where $\bar{B} = 3^{1/2}V\dot{\epsilon}/3\Omega$ and $C = 27A\mu\Omega D_v/8r^2kT$. In the case of grain boundary diffusion, C in the above equation should be replaced by $27A\mu\Omega D_{GB}\delta/4r^3kT$.

If Equation 14 is solved by putting $n = 0$ for $t = 0$ under a constant strain rate (more rigorously, under a constant plastic strain rate), the following solution is obtained:

$$n = \frac{\bar{B}}{C}(1 - e^{-Ct}) \quad (15)$$

Since $\epsilon = \dot{\epsilon}t$ for a constant strain rate, n is also given by

$$n = \frac{\bar{B}}{C}(1 - e^{-C\epsilon/\dot{\epsilon}}) \quad (15)'$$

Substituting the above equation into Equations 3 and 6,

$$\epsilon^* = \frac{\dot{\epsilon}}{C}(1 - e^{-C\epsilon/\dot{\epsilon}}) \quad (16)$$

$$\Delta\sigma = \frac{3}{2}A\mu\frac{f}{1-fB}\cdot\frac{\dot{\epsilon}}{C}(1 - e^{-C\epsilon/\dot{\epsilon}}) \quad (17)$$

Therefore, the work hardening rate of the material, θ ($= d(\Delta\sigma)/d\epsilon$), is derived from Equation 17 and is written as follows:

$$\theta = \frac{3}{2}A\mu\frac{f}{1-fB}e^{-C\epsilon/\dot{\epsilon}} \quad (18)$$

3. Experimental results

Tensile tests were performed on two kinds of aged 21Cr–4Ni–9Mn austenite steels with $M_{23}C_6$ carbides under a constant strain rate of $1.33 \times 10^{-4}\,sec^{-1}$ in the temperature range from 306 K (33° C) to 1073 K (800° C). The 21Cr–4Ni–9Mn

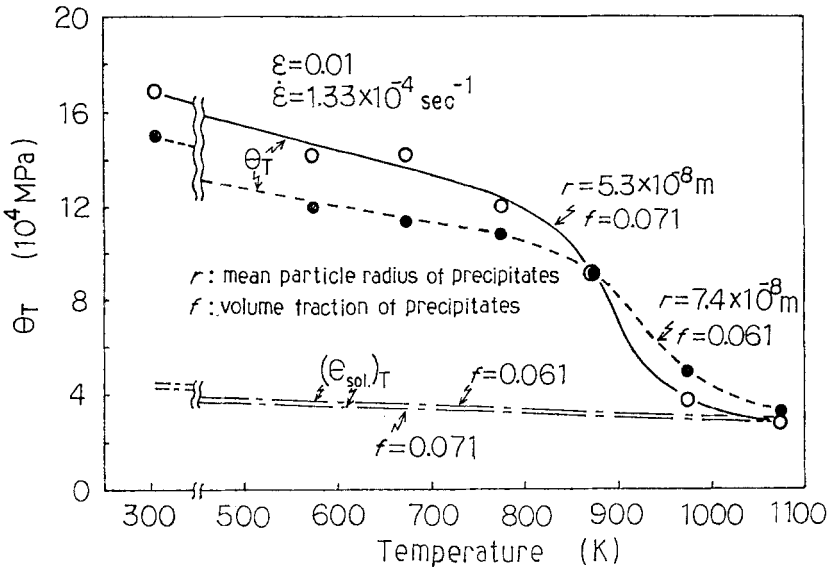

Figure 2 The work hardening rate against temperature in austenitic 21Cr–4Ni–9Mn steel.

austenite steel in this study has the basic components of 0.51% C, 0.40% N, 20.22% Cr, 3.90% Ni and 8.75% Mn. The steel was water-quenched after solution heating for 3.6 ksec (1 h) at 1473 K (1200° C). Then, the simple ageing treatment, which consisted of heating for 108 ksec (30 h) at 1023 K (750° C) and subsequent air-cooling, was employed to develop 7.1 vol% of $M_{23}C_6$ carbides (particle radius of 5.3×10^{-8} m). The two-step ageing treatment which involved ageing for 108 ksec at 1273 K (1000° C) after pre-ageing for 108 ksec at 973 K (700° C) was also performed to develop 6.1 vol% of the precipitates (particle radius of 7.4×10^{-8} m). Further, other kinds of precipitates were not detected in this steel using transmission electron microscopy. Fig. 2 shows the work hardening rate at $\epsilon = 0.01$ in the rapid hardening region, θ_T, against test temperature. The temperature dependence of work hardening was also found in solid solution without precipitates. A considerable contribution of solid solution hardening can be expected in this steel with a large amount of carbon and nitrogen [9]. The solid solution hardening is proportional to the square root of the concentration of solute atoms in the matrix [10]. The work hardening rate of solid solution with about 3.9 at% carbon and nitrogen, θ_{st}, was experimentally obtained in a tensile test at room temperature (306 K). The contribution of solid solution hardening at elevated temperatures, $(\theta_{sol.})_T$, was then calculated for aged steel using the following equation. The result of this calculation is also shown in Fig. 2.

$$(\theta_{sol.})_T = \theta_{st} \frac{\mu_T}{\mu_{RT}} \left(\frac{c_T}{c_0}\right)^{1/2} \tag{19}$$

where c_0 and c_T are the concentrations of solute atoms in the matrix for the solid solution and for aged steel, respectively. These can be obtained from the measurement of the lattice parameter of the austenite matrix by means of X-ray diffraction, using the relationship between lattice parameter and dissolved carbon plus nitrogen content in the matrix of this steel [11]. Those values used in the calculation were $c_T = 2.32$ at% for the steel with $f = 0.061$, 2.06 at% for that with $f = 0.071$ and $c_0 = 3.91$ at% for solid solution. μ_{RT} and μ_T are the rigidity of the matrix at room temperature and that at elevated temperatures, respectively. The rigidity and Poisson's ratio of AISI316 steel at elevated temperatures were used in the calculation of this study [12], since those values are still unknown for 21Cr–4Ni–9Mn steel.

Fig. 3 shows the temperature dependence of the net work hardening rate due only to the presence of precipitate particles. The values in this figure were obtained by subtracting the contribution of solid solution hardening calculated by Equation 19 from the experimental values and then these were temperature-compensated. Change in the work hardening rate occurs in the temperature range from about 770 to 1100 K. A decrease in the work hardening rate can be observed at a lower temperature and the extent of it is larger in the steel with precipitates of the smaller particle size in this figure.

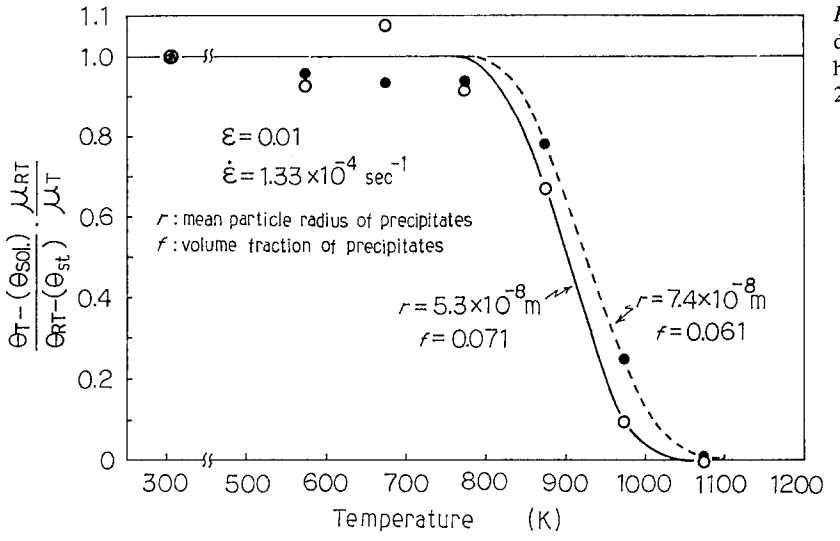

Figure 3 Temperature dependence of the normalized work hardening rate in austenitic 21Cr–4Ni–9Mn steel.

4. Discussions

4.1. Work hardening rate and stress–strain curve

Fig. 4 shows the result of calculation of Equation 18 and the temperature-compensated work hardening rate for $\epsilon = 0.01$. It was assumed from the result of the tensile test at room temperature that the values of rigidity, μ', and Poisson's ratio, ν', of $M_{23}C_6$ carbides are the same as those of the austenite matrix ($\mu' = \mu$, $\nu' = \nu$), and therefore, $A = 2(7 - 5\nu)/15(1 - \nu)$ and $B = 1$. The activation energy and diffusion constant for self-diffusion in γ-Fe [$Q = 270\,\mathrm{kJ\,mol^{-1}}$ (64.5 kcal $\mathrm{mol^{-1}}$), $D_{v_0} = 1.8 \times 10^{-5}\,\mathrm{m^2\,sec^{-1}}$] [13], and the value of the activation energy, $Q = 253\,\mathrm{kJ\,mol^{-1}}$, were used in the numerical calculation. The latter value of Q lies between the apparent activation energy for creep ($236\,\mathrm{kJ\,mol^{-1}}$) of the steel used in this study [14] and the activation energy for self-diffusion in γ-Fe. Good agreement is found between the experimental and calculated work hardening rates for $Q = 253\,\mathrm{kJ\,mol^{-1}}$, while the calculated value for $Q = 270\,\mathrm{kJ\,mol^{-1}}$ is slightly higher. The particle size dependence of the work hardening rate at elevated temperatures can be also satisfactorily explained by the result of the theoretical calculation in this study. The change in the actual work hardening rate was observed in a slightly wider temperature range compared with the result of calculation. This can be attributed primarily to the particle size distribution of precipitates, as pointed out by Matsuura [3], and secondly to the fact that the climb and annihilation process of individual dislocation loops is not considered in the present calculation.

Figs. 5 and 6 show the calculated and exper-

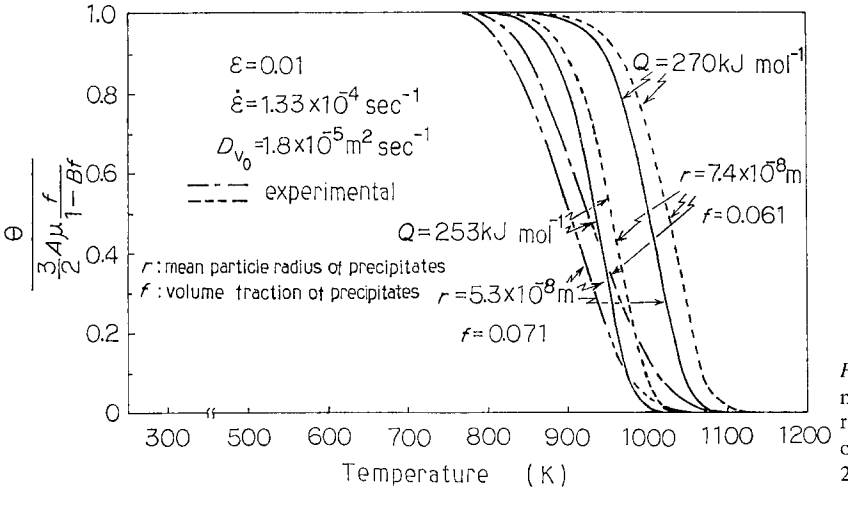

Figure 4 Comparison of the normalized work hardening rate by calculation with that of experiment in austenitic 21Cr–4Ni–9Mn steel.

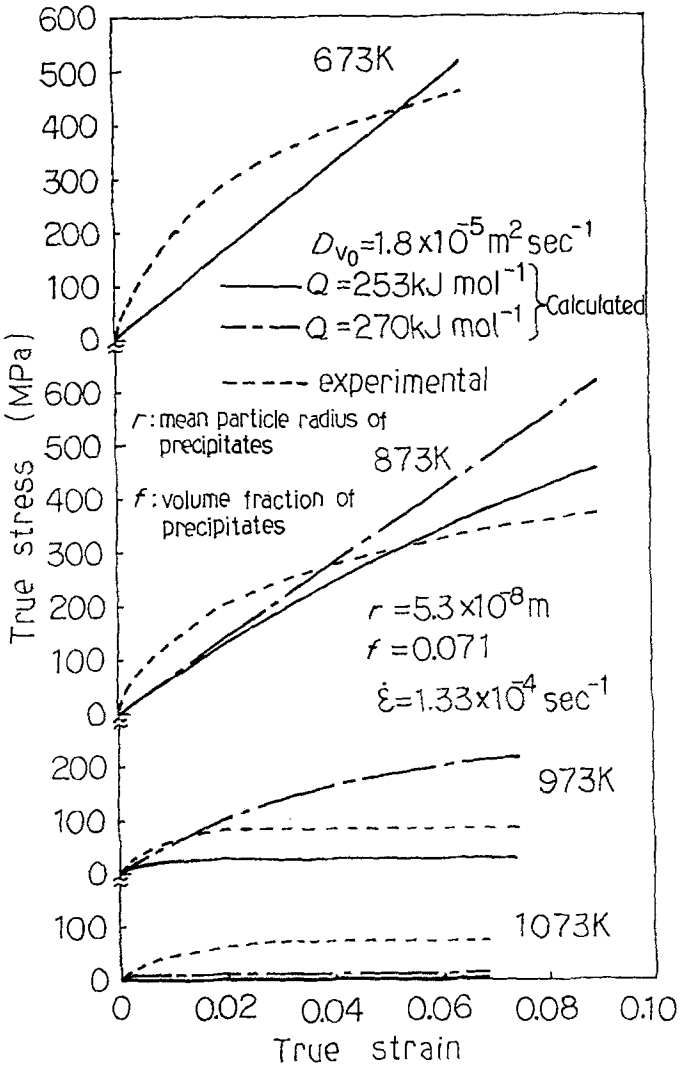

Figure 5 The calculated stress–strain curve and the experimental one in austenitic 21Cr–4Ni–9Mn steel ($r = 5.3 \times 10^{-8}$ m, $f = 0.071$).

imental stress–strain curves of the steels after yielding. There is good agreement between the calculated and experimental curves for $Q = 253\,kJ\ mol^{-1}$. As already described, the contribution of solid solution hardening is also expected in this steel. However, the stress–strain curve of the solid solution in the high-temperature range could not be obtained in this study, because carbon and nitrogen have a strong tendency to form precipitates as the sample is heated up to and maintained at the test temperatures. Therefore, the contribution of solid solution hardening to the work hardening behaviour of the material was estimated by Equation 20 based on the result of the tensile test on the solid solution at room temperature,

$$\sigma_s = \frac{\mu_T}{\mu_{RT}}\left(\frac{c_T}{c_0}\right)^{1/2}(940\epsilon^{0.066} - 564)(\text{MPa}) \quad (20)$$

where $\epsilon \geqq 0.0005$. Figs. 7 and 8 show the calculated stress–strain curves in which the contribution of solid solution hardening is taken into account, and the experimental curves. Much better agreement is found between the result of the calculation and that of experiment in these figures than in Figs. 5 and 6. The work hardening rate of the steels increases with an increase of strain rate, as shown in Fig. 9, although the contribution of solid solution hardening is not involved in the calculation. This increase is greater in the steel with precipitates of larger particle size.

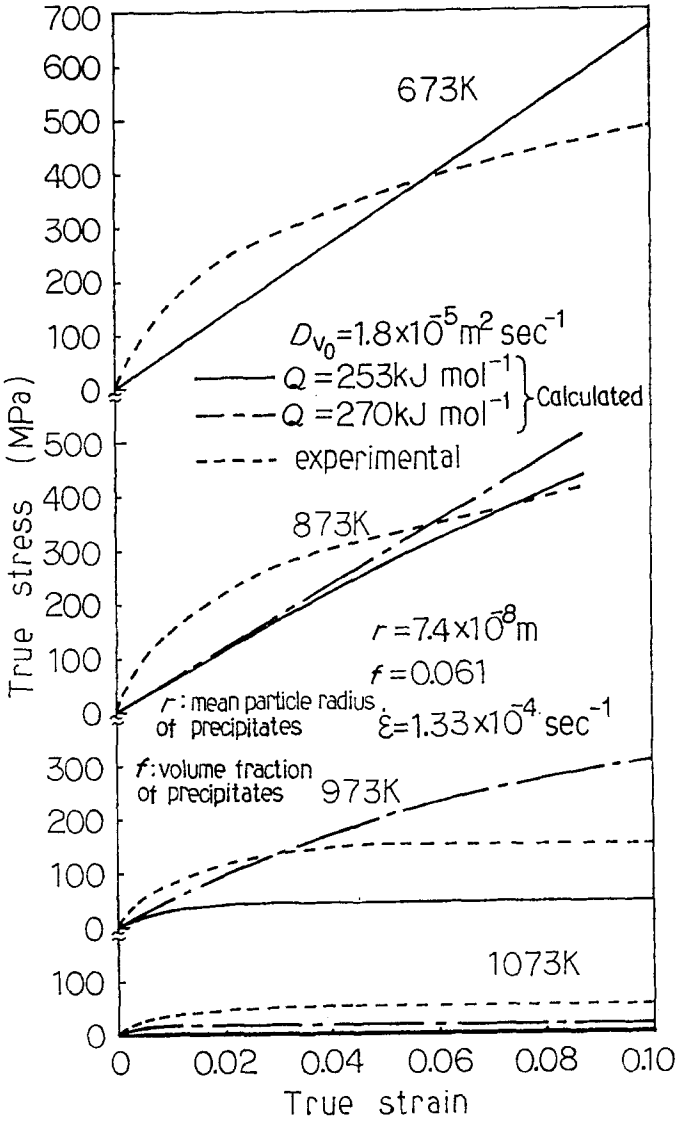

Figure 6 The calculated stress–strain curve and the experimental one in austenitic 21Cr–4Ni–9Mn steel ($r = 7.4 \times 10^{-8}$ m, $f = 0.061$).

Thus, in this study, the temperature and particle size dependence of the work hardening rate in metallic materials with spherical second-phase particles can be explained by the continuum mechanics model without any ambiguous parameters, even if the annihilation process of each dislocation loop around precipitates is quite unknown.

4.2. Internal stress during high-temperature creep

The continuum mechanics model in this study can be also applied to the interpretation of internal stress in the steel with spherical precipitates during high-temperature creep. The work hardening is balanced with the recovery in steady-state creep, and therefore, $d(\Delta\sigma)/d\varepsilon = 0$. Using Equation 17, the amount of work hardening, $\Delta\sigma$, is given by

$$\Delta\sigma = \frac{7-5\nu}{5(1-\nu)}\,\mu\,\frac{f}{1-f}\,\frac{\dot{\epsilon}}{C} \qquad (21)$$

The internal stress during creep is given by $\Delta\sigma + \sigma_0$, since the Orowan stress, σ_0, is approximately $2\mu b/l$, where l is the mean interparticle spacing and b the magnitude of the Burgers' vector, respectively. Fig. 10 shows the internal stress values, σ_i, which were experimentally obtained by one of the authors [14], and the calculated values of $\Delta\sigma + \sigma_0$ for $r = 5.3 \times 10^{-8}$ m ($l = 1.06 \times 10^{-7}$ m) by the steady-state creep model. The experimental value of μ, 65 GPa, in this steel was used in this calculation. The calculated internal stress, $\Delta\sigma + \sigma_0$, and the experimental value, σ_i, are almost the same

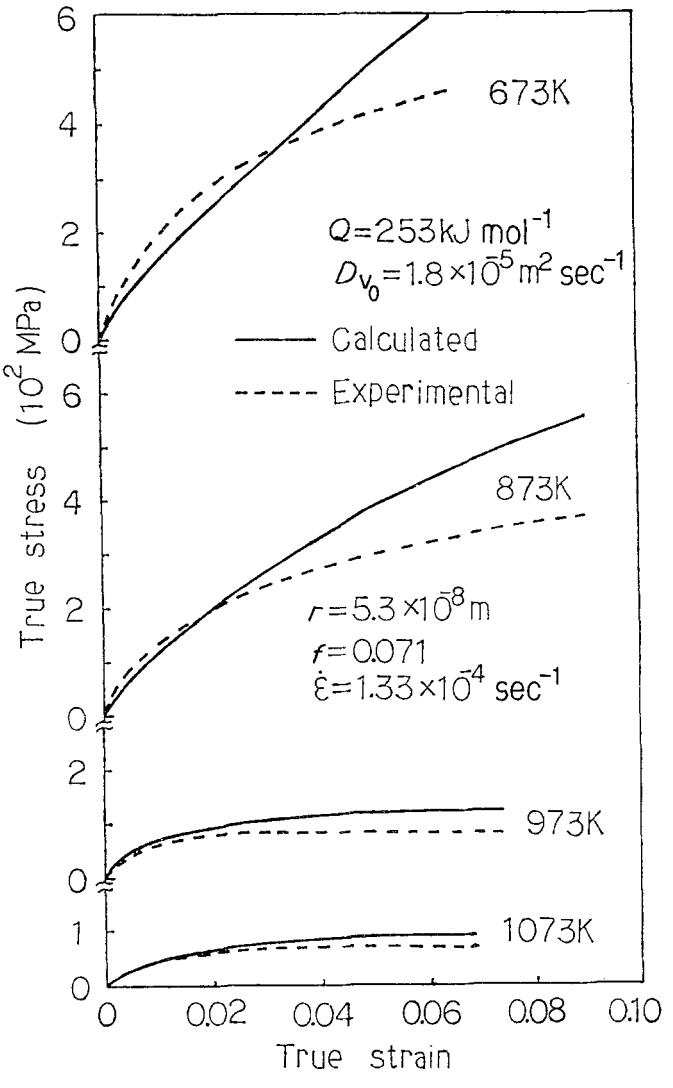

Figure 7 The calculated stress–strain curve which involves the contribution of solid solution hardening and the experimental one in austenitic 21Cr–4Ni–9Mn steel ($r = 5.3 \times 10^{-8}$ m, $f = 0.071$).

and independent of the steady-state creep rate. $\Delta\sigma$ is very small compared with σ_0, while it increases with an increase in the steady-state creep rate. The creep rate is extremely high and decreases rapidly with an increase of time in the transient creep regime. Such a path-dependence of creep deformation can also be taken into account by numerically integrating Equation 14 by the Runge–Kutta method. Fig. 11 shows an example of the result of calculation. The value of $\Delta\sigma/\sigma_0$ decreases abruptly with an increase of time to reach the calculated value shown in Fig. 10, while it is large in the early stage of creep.

The continuum mechanics model in this study incorporates the recovery effect by diffusion of atoms and involves no parameters whose physical meaning is ambiguous. It can explain quantitatively the high-temperature deformation of the metallic material with second-phase particles, using numerical values of particle size and volume fraction of the second phase, and physical constants. Further, it is also applicable to the prediction of work hardening behaviour for the design of materials.

5. Conclusion

A continuum mechanics model without any ambiguous parameters was developed to explain the temperature and particle size dependence of the work hardening behaviour of a metallic material with non-deforming second-phase particles at elevated temperatures where the dynamic recovery due to volume diffusion of atoms is predominant. Good agreement was found between

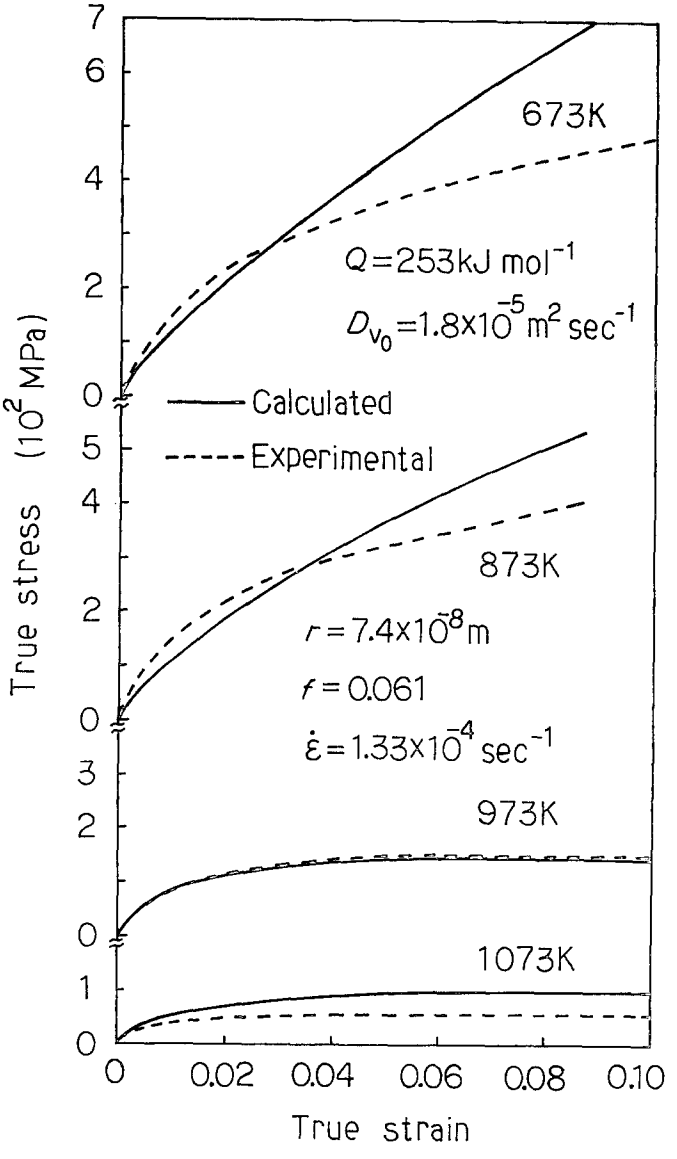

Figure 8 The calculated stress–strain curve which involves the contribution of solid solution hardening and the experimental one in austenitic 21Cr–4Ni–9Mn steel ($r = 7.4 \times 10^{-8}$ m, $f = 0.061$).

the result of calculation based on this model and experimental results. The results obtained are summarized as follows.

1. The differential equation of the primary reaction was derived, based on the dynamic recovery model that diffusion of atoms in a matrix causes the change in the Gibbs free energy, and that the climb and annihilation of dislocation loops occurs as a result of accommodation of the misfit strain between a precipitate particle and the matrix.

2. The differential equation can be solved when the strain rate is constant. As far as the temperature and particle size dependence of the work hardening behaviour were concerned, good agreement was confirmed between the result of calculation which involved the contribution of solid solution hardening and that of the tensile test on an austenitic heat-resisting steel with $M_{23}C_6$ carbides.

3. This model is also applicable to the interpretation of the internal stress in high-temperature creep. The calculated internal stress during steady-state creep was almost the same as the experimental value of an austenitic heat-resisting steel with $M_{23}C_6$ carbides. Its steady-state creep rate dependence also coincided with the experimental result. The theoretical internal stress when the path dependence of creep deformation was taken into account reached the calculated value based on the

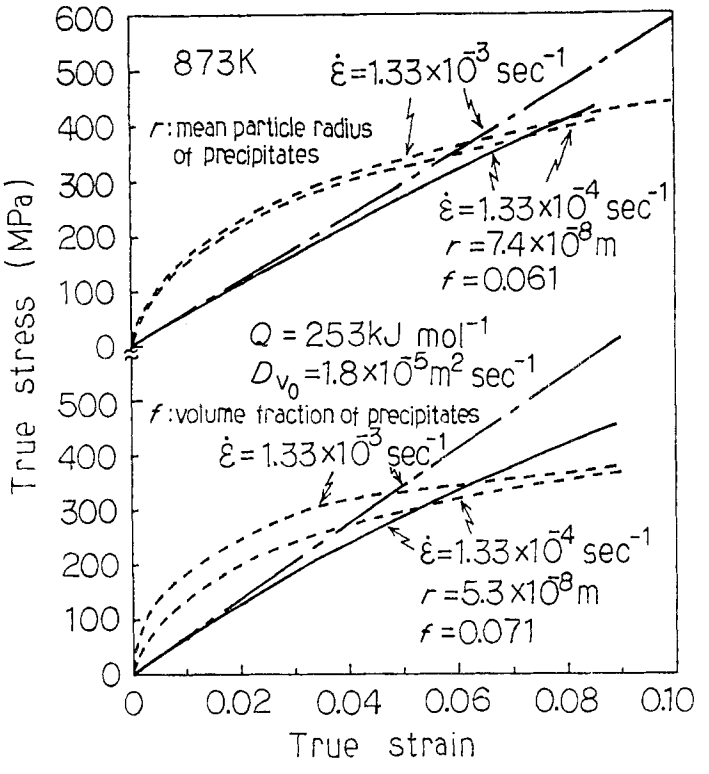

Figure 9 Strain rate dependence of the work hardening behaviour in austenitic 21Cr–4Ni–9Mn steel.

steady-state creep model after long term creep, while the amount of work hardening was large in the early stage of creep.

4. The continuum mechanics model in this study involves no ambiguous parameters. Therefore, the work hardening behaviour of the metallic material with non-deforming second-phase particles at elevated temperatures can be calculated using physical constants, if the particle size and volume fraction of the second phase are known. This model is also applicable to the prediction of high-temperature deformation of the material with precipitates or dispersoids.

Acknowledgements

The author wishes to express thanks to Professor K. Matsuura of Yamagata University for his assistance in this study.

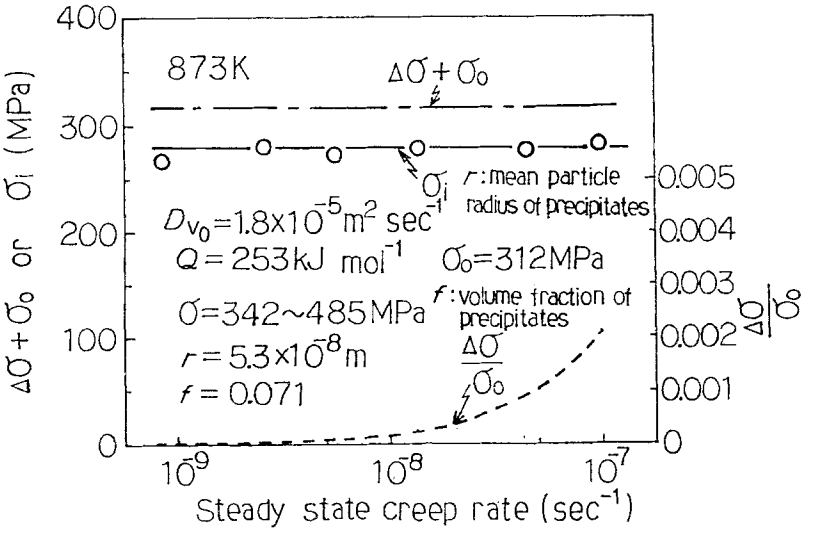

Figure 10 Comparison of the calculated internal stress with the experimental value during steady-state creep in austenitic 21Cr–4Ni–9Mn steel.

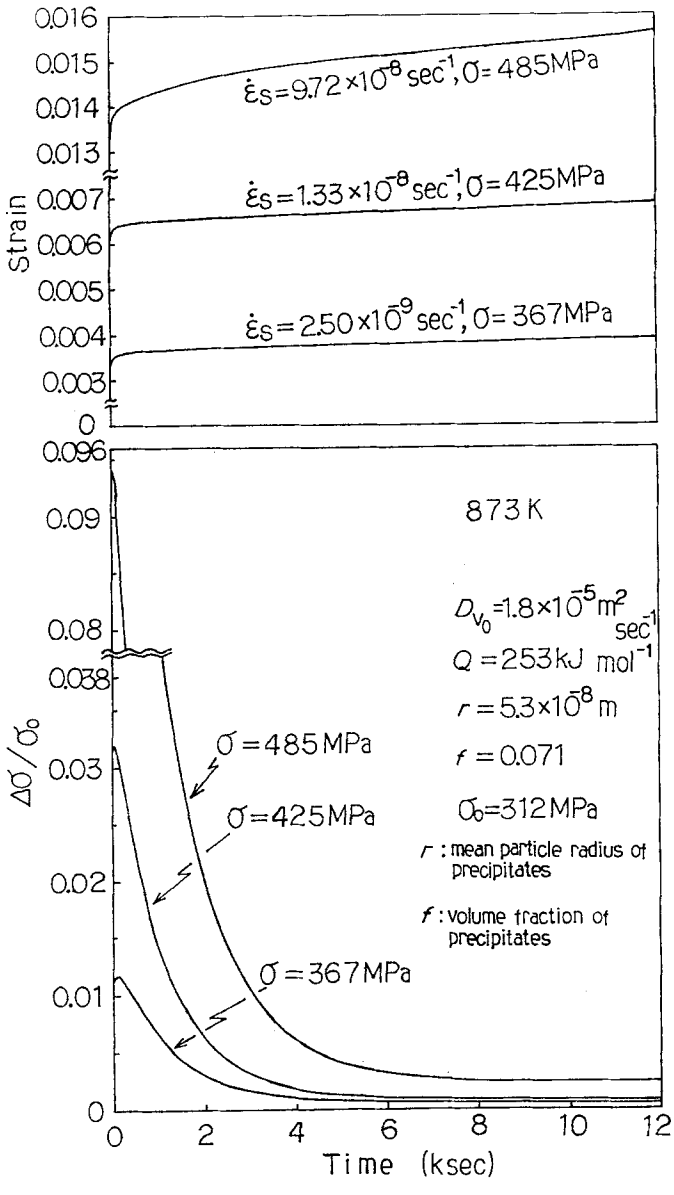

Figure 11 Changes in the amount of work hardening and creep strain with time in austenitic 21Cr–4Ni–9Mn steel.

References

1. T. MORI and H. TOKUSHIGE, *Acta Metall.* **25** (1977) 635.
2. M. OKABE and T. MORI, *ibid.* **27** (1979) 1373.
3. K. MATSUURA, *J. Japan Inst. Met.* **44** (1980) 346.
4. *Idem, Acta Metall.* **29** (1981) 643.
5. M. F. ASHBY, Proceedings of the 2nd International Conference on the Strength of Metals and Alloys, Vol. II (American Society for Metals, 1970) p. 534.
6. K. TANAKA and T. MORI, *Acta Metall.* **18** (1970) 931.
7. J. D. ESHELBY, *Proc. R. Soc. (Lond.)* **A241** (1957) 376.
8. T. MORI, M. OKABE and T. MURA, *Acta Metall.* **28** (1980) 319.
9. H. FUJITA, M. TANAKA, O. MIYAGAWA and T. SAKAKI, *Trans. Japan Soc. Mech. Engrs.* **45** (1979) 1451.
10. R. HASHIGUCHI and T. CHIKAZUMI, "Strength of Crystals", Series of Materials Science, Vol. 3 (Asakura, Tokyo, 1968) p. 47.
11. M. TANAKA, O. MIYAGAWA and D. FUJISHIRO, *J. Japan Inst. Met.* **41** (1977) 11.
12. A. MURAMATSU, *J. Japan Soc. Mech. Engrs.* **68** (1965) 1623.
13. S. KODA, "Metal Physics" (Corono, Tokyo, 1978) p. 120.
14. M. TANAKA and H. FUJITA, *J. Japan Inst. Met.* **45** (1981) 1187.

Received 29 November 1983
and accepted 2 February 1984